ResearchGate

See discussions, stats, and author profiles for this publication at: https://www.researchgate.net/publication/1835284

Helix Formation and Folding in an Artificial Peptide

ARTICLE *in* THE JOURNAL OF CHEMICAL PHYSICS · MAY 2002

Impact Factor: 2.95 · DOI: 10.1063/1.1489419 · Source: arXiv

CITATIONS
32

READS
16

2 AUTHORS:

Nelson A. Alves
University of São Paulo
44 PUBLICATIONS **630** CITATIONS
SEE PROFILE

Ulrich H E Hansmann
University of Oklahoma
213 PUBLICATIONS **4,801** CITATIONS
SEE PROFILE

All in-text references underlined in blue are linked to publications on ResearchGate, letting you access and read them immediately.

Available from: Ulrich H E Hansmann
Retrieved on: 26 January 2016

arXiv:cond-mat/0205559v1 [cond-mat.stat-mech] 27 May 2002

Helix Formation and Folding in an Artificial Peptide

Nelson A. Alves*
Departamento de Física e Matemática, FFCLRP Universidade de São Paulo. Av. Bandeirantes 3900. CEP 014040-901 Ribeirão Preto, SP, Brazil

Ulrich H.E. Hansmann †
Department of Physics, Michigan Technological University, Houghton, MI 49931-1291, USA
(February 1, 2008)

We study the relation between α-helix formation and folding for a simple artificial peptide, Ala_{10}-Gly_5-Ala_{10}. Our data rely on multicanonical Monte Carlo simulations where the interactions among all atoms are taken into account. The free-energy landscape of the peptide is evaluated for various temperatures. Our data indicate that folding of this peptide is a two-step process: in a first step two α-helices are formed which afterwards re-arrange themselves into a U-like structure.

I. INTRODUCTION

The mechanism by which a large class of proteins folds spontaneously into a unique globular shape [1] has remained elusive. Significant new insight was gained over the last few years from the studies of minimal protein models. For instance, energy landscape theory and funnel concept [2,3] proved to be powerful tools for description of the general characteristics of folding not only in minimalistic protein models but also for real proteins [4,5]. However, many questions on the details of the folding process remain to be solved. For instance, folding of proteins involves one or more transitions between different thermodynamic states. The role of these transitions in the folding process is an active area of research. An important example for these transitions is the formation of secondary structure elements. For the case of α-helices it is long known that there is a sharp transition towards a random coil state when the temperature is increased. The characteristics of this so-called helix-coil transition have been studied extensively [6], most recently in Refs. [7–12]. In this paper, we research the relation between helix-coil transition and folding.

For this purpose, we have studied an artificial peptide, Ala_{10}-Gly_5-Ala_{10}, in a detailed representation where the interactions between all atoms are taken into account. Multicanonical simulations [13] with large statistics are used to evaluate the free energy landscape of our peptide at different temperatures. The encountered transitions are further investigated by partition zeros analysis which allows to characterize "phase transitions" in small systems [14]. Quantities such as the energy, specific heat, helicity and susceptibility were calculated as function of temperature. We have neglected in the simulations the interaction of our artifical peptide with the surrounding solvent. While this is certainly a crude approximation, it allows us not only to relate our results to our previous studies on helix-coil transition in poly-alanine that also relied on gas-phase simulations [8–10], but also to study the extend to that secondary structure formation and folding are determined by intrinsic properties of the peptide. Our data suggest that the peptide in gas-phase folds in a two-step process: in a first step two α-helices are formed in what amounts to a first order transition. Afterwards these helices re-arrange themselves into a U-like structure. The second step has the characteristics of a second order transition.

II. METHODS

Our investigation of Ala_{10}-Gly_5-Ala_{10} is based on a detailed, all-atom representation of that peptide. The interaction between the atoms is described by a standard force field, ECEPP/2, [16] (as implemented in the program package SMMP [17]) and is given by:

$$E_{tot} = E_C + E_{LJ} + E_{HB} + E_{tor}, \tag{1}$$

$$E_C = \sum_{(i,j)} \frac{332 q_i q_j}{\epsilon r_{ij}}, \tag{2}$$

*E-mail: alves@quark.ffclrp.usp.br
†hansmann@mtu.edu, to whom all correspondence should be addressed

$$E_{LJ} = \sum_{(i,j)} \left(\frac{A_{ij}}{r_{ij}^{12}} - \frac{B_{ij}}{r_{ij}^{6}} \right), \tag{3}$$

$$E_{HB} = \sum_{(i,j)} \left(\frac{C_{ij}}{r_{ij}^{12}} - \frac{D_{ij}}{r_{ij}^{10}} \right), \tag{4}$$

$$E_{tor} = \sum_{l} U_l \left(1 \pm \cos(n_l \chi_l)\right). \tag{5}$$

Here, r_{ij} (in Å) is the distance between the atoms i and j, and χ_l is the l-th torsion angle. The peptide bond angles were set to their common value $\omega = 180°$. We do not include explicitly the interaction of the peptide with the solvent into our simulations and set the dielectric constant ϵ equal to 2. Since the charges at peptide termini are known to reduce helix content [15], we removed them by taking a neutral NH_2– group at the N-terminus and a neutral –COOH group at the C-terminus.

Simulation of detailed protein models where the interaction between all atoms are taken into account are extremely difficult. This is because the various competing interactions within the molecule lead to an energy landscape characterized by a multitude of local minima separated by high energy barriers. Hence, in the low-temperature region, canonical Monte Carlo or molecular dynamics simulations will tend to get trapped in one of these minima and the simulation will not thermalize within the available CPU time. One example of the new and sophisticated algorithms [18] that allow to overcome this difficulty are *generalized-ensemble* techniques [19,20], and it is one of these techniques, multicanonical sampling [13], that we used for our investigations.

In the multicanonical algorithm [13] conformations with energy E are assigned a weight $w_{mu}(E) \propto 1/n(E)$. Here, $n(E)$ is the density of states. A simulation with this weight will lead to a uniform distribution of energy:

$$P_{mu}(E) \propto n(E)\, w_{mu}(E) = \text{const}\ . \tag{6}$$

This is because the simulation generates a 1D random walk in the energy space, allowing itself to escape from any local minimum. Since a large range of energies are sampled, one can use the reweighting techniques [21] to calculate thermodynamic quantities over a wide range of temperatures T by

$$< \mathcal{A} >_T \;=\; \frac{\int dx\ \mathcal{A}(x)\ w^{-1}(E(x))\ e^{-\beta E(x)}}{\int dx\ w^{-1}(E(x))\ e^{-\beta E(x)}}\ , \tag{7}$$

where x stands for configurations.

Note that unlike in the case of canonical simulations the weights

$$w(E) = n^{-1}(E) = e^{-S(E)} \tag{8}$$

are not a priori known. Instead estimators for these weights have to be determined by an iterative procedure [22,12]. In our case we needed 500,000 sweeps for the weight factor calculations. All thermodynamic quantities were then estimated from one production run of $8,000,000$ Monte Carlo sweeps which followed 10,000 sweeps for thermalization. Our simulations were started from completely random initial conformations (Hot Start) and one Monte Carlo sweep updates every torsion angle of the peptide once. At the end of every 10th sweep we stored the ECEPP/2 energies $E_{tot}, E_C, E_{LJ}, E_{hb}$ and E_{tor} of the conformation, the corresponding number n_H of helical residues and end-to-end distance d_{e-e}. Here, we follow previous work [23] and consider a residue as helical if its backbone angle (ϕ, ψ) are within the range $(-70° \pm 20°, -37° \pm 20°)$.

Using the results of our generalized-ensemble simulation, we explored for various temperatures the free energies

$$G(n_H, d_{e-e}) = -k_B T \log P(n_H, d_{e-e})\ . \tag{9}$$

Here, $P(n_H, d_{e-e})$ is the probability to find a peptide conformation with values ℓ, d_{e-e} (at temperature T). We chose the normalization so that the lowest value of $G(n_H, d_{e-e})$ is set to zero for each temperature.

We finally used that the multicanonical algorithm allows us to calculate estimates for the spectral density:

$$n(E) = P_{mu}(E) w_{mu}^{-1}(E)\ . \tag{10}$$

We can therefore construct the corresponding partition function for our all-atom model of Ala_{10}-Gly_5-Ala_{10} from these estimates by

$$Z(\beta) = \sum_E n(E) e^{-\beta E}, \tag{11}$$

with β the inverse temperature, $\beta = 1/k_B T$. The complex solutions of the partition function determine the critical behavior of the model and were also studied by us.

III. RESULTS AND DISCUSSION

Our peptide, Ala_{10}-Gly_5-Ala_{10}, is build up out of two chains of each 10 alanine residues connected by 5 glycine residues. In previous work [23,8,9] we could show that polyalanine has a pronounced transition between a disordered coil phase and an ordered state in which the polymer forms an α-helix. For this reason, we expect formation of α-helices in our peptide, and the average number of helical residues $< n_H >$ is therefore one of the quantities that we have measured. $< n_H >$ is displayed in Fig. 1 as a function of temperature, and we observe in this plot two temperature regions. At high temperature, few residues are found with backbone dihedral angles (ϕ, ψ) typical for an α-helix. On the other hand, at low temperatures we observe helix-formation, and almost all of the alanine residues are part of an α-helix, i.e. have backbone dihedral angles (ϕ, ψ) in the range $(-70° \pm 20°, -37° \pm 20°)$. The transition between the two temperature regions is sharp indicating the existence of a helix-coil transition. The transition temperature T_{hc} can be determined from the corresponding peak in the susceptibility

$$\chi(T) = < n_H^2(T) > - < n_H(T) >^2 , \tag{12}$$

which is ploted in the inset of Fig. 1, and we find the transition temperature $T_{hc} = 485 \pm 5$ K.

In previous work [23,12] we could show that in polyalanine the formation of α-helices is related to a gain in potential energy. For this reason, we display in Fig. 2 the average total ECEPP/2 energy $< E_{tot} >$ and the thermodynamic averages of partial energies $< E_C >$, $< E_{LJ} >$, $< E_{hb} >$ and $< E_{tor} >$ of Ala_{10}-Gly_5-Ala_{10} as a function of temperature. As expected, we observe around our transition temperature T_{hc} a sharp decrease in the potential energy $< E_{tot} >$ that is due to a corresponding decrease in the Coulomb energy $< E_C >$, Lennard-Jones energy $< E_{LJ} >$ and hydrogen-bond energy $< E_{hb} >$. The change in $< E_{tot} >$ with temperature can be described by the specific heat

$$C(T) = \beta^2 \ \frac{< E_{tot}^2 > - < E_{tot} >^2}{25}, \tag{13}$$

which we display in Fig. 3. A pronounced change in energy with temperature corresponds to a peak in the specific heat. As one can see from Fig. 3, we observe indeed a pronounced peak in the specific heat at a temperature $T = 480 \pm 10$ K that is consistent with $T = 485 \pm 5$ K, the temperature where the peak in the susceptibility is located. Combining both values we obtain as our final estimate for the helix-coil transition temperature $T_{hc} = 483 \pm 8$. However, we find in Fig. 3 also a second, smaller peak in the specific heat at the lower temperature $T_f = 265 \pm 7$ K indicating yet another transition.

The sharp decrease in potential energy corresponding to this second peak is clearly visible in Fig. 2 for the total energy $< E_{tot} >$, however, not for all of the partial energies. Only the Lennard-Jones term $< E_{LJ} >$ exhibits also a signal for the second transition at T_f. This energy term depends strongly on the overall size of the molecule and the change in this quantity indicates a transition between extended and compact structures. Hence, we conjecture that the second peak in specific heat at the lower temperature T_f is related to a transition between extended and compact structures. A possible measure for such a change is the average end-to-end distance $< d_{e-e} >_T$. We define here $< d_{e-e} >$ as the distance between N of Ala_1 and O of Ala_{25}, and plot this quantity in Fig. 4. We observe that this quantity decreases with decreasing temperature. Below the helix-coil transition T_{hc} the decrease slows down and the curve becomes almost flat at a value of $< d_{e-e} > \approx 10$ Å indicating that there is little further change in the compactness of the molecule. However, at temperature T_f the end-to-end distance decreases again sharply towards a new value $< d_{e-e} > = 6.1$ Å. Hence, T_f marks the folding of the molecule into a defined compact structure with the two terminal ends of the peptide close together.

The transition between extended and a more compact structure can also be seen when we display the free energy landscape of our peptide as a function of helicity n_H and end-to-end distance d_{e-e}. At the temperature $T = 480$ K (which is essentially the helix-coil transition temperature $T_{hc} = 483 \pm 8$ K) the free energy landscape (displayed in Fig. 5a) is flat over a large range of values of n_H and d_{e-e}. The $3k_BT$ contour line surrounds a region where the helicity can take values between $0 \leq n_H \lesssim 20$ and the end-to-end distance values between $3 \lesssim d_{e-e} \lesssim 40$, allowing the system to move freely between extended and compact configurations, and between helical and coil configurations. On the

other hand, at the second and lower temperature $T = 270$ K (which is essentially the folding transition temperature $T_f = 265 \pm 7$ K) the free energy grows rapidly with decreasing helicity n_H favoring configuration in a small strip with $15 \lesssim n_H \lesssim 25$. Hence, the plot of the free energy landscape in Fig. 5b is limited to values $12 \lesssim n_H \lesssim 25$ of the helicity. Here, two regions of minimal free energy can be seen (marked by the 3 k_BT contour lines). The first minima is found at values of d_{e-e} between 5 and 10 Å and $15 \leq n_H \leq 20$ characterising compact structures. A second region with slightly lower free energy (see the 1 k_BT contour line) is found at much larger values of d_{e-e} between 35 and 40 Å and $20 < n_H \leq 25$ indicating a long stretched α-helix. Both local free energy minima are separated by free energy barriers of ≈ 8 k_BT that can be overcome by thermal fluctuations. On the other hand, configurations with helicity $n_H < 10$ are suppressed by free energy differences of more than 30 k_BT.

Examples for the structures corresponding to the two free energy minima are plotted in Fig. 6. The first one, displayed in Fig. 6a is the configuration with lowest energy ever found in our multicanonical simulation of 8,000,000 sweeps and corresponds to the region in the free-energy landscape at values of d_{e-e} between 5 and 10 Å and $15 \leq n_H \leq 20$. This conformation ('A') consists out of two helixes (made up out of the alanine residues) connected by a turn (build out of the flexible glycine residues) towards a U-turn-like structure that is consistent with the small value of the end-to-end distance d_{e-e} observed in Fig. 4 for temperatures below T_f. For reference we show in Fig. 6b also the configuration ('B') where all 25 residues are part of an α-helix and which corresponds to the second local free-energy minimum in Fig. 5b at values of d_{e-e} between 35 and 40 Å and $20 < n_H \leq 25$. The dihedral angles of both configurations are listed in Table 1. Fig. 7 displays the frequency of both configurations as a function of temperature. For $T > T_{hc}$ neither configuration 'A' nor 'B' are observed. Below that temperature both structures appear with similar probability as long as the temperature is higher than T_f. At $T = T_f$ the probability to find the maximal helical structure 'B' is with ≈ 30 % highest and decreases after that with decreasing temperature. On the other hand, the frequency for the U-turn structure 'A' continues to grow with decreasing temperature. This different behavior is due to the energy differences between both structures. The minimal energy conformation 'A' has with $E_{tot} = -34.7$ Kcal/mol a 10.8 Kcal/mol lower potential energy than the extended helix conformation 'B' ($E_{tot} = -23.9$ Kcal/mol). This difference is mainly due to the Lennard-Jones terms: $E_{LJ} = -132.5$ Kcal/mol for 'A' vs. $E_{LJ} = -118.9$ Kcal/mol for 'B'. The gain in E_{LJ} is in part compensated by the hydrogen-bonding terms: $E_{hb} = -30.2$ Kcal/mol for 'A' vs. $E_{hb} = -34.7$ Kcal/mol for 'B'. Coulomb and torsion energies differed little between the two configurations: $E_C = 126.7$ Kcal/mol and $E_{tor} = 1.3$ Kcal/mol for conformation 'A' vs. $E_C = 126.4$ Kcal/mol and $E_{tor} = 3.3$ Kcal/mol for conformation 'B'.

It is an interesting question whether our two observed transitions (occuring in a finite and small system) can be related to phase transitions which in a strict sense are defined only for macroscopic (that is very large) systems. In order to study this question we have calculated the complex zeros $\beta \to \mathrm{Re}(\beta) + i\tau$ of the partition function $Z(\beta)$ of our molecule. In the case of a temperature driven phase transition, we expect that the complex zeros β_j, $(j = 1, 2, ...)$ (or at least the ones close to the real axis) condense for large enough system size on a single line. As the system size increases, those zeros will move towards the positive real β-axis and the corresponding value is for large system size the inverse of the physical critical temperature T_c. Crucial information on phase transitions can be obtained from the way in which the first zero approaches the real β-axis. However, such an analysis depends on the extrapolation towards the infinite large system and does not allow characterization of the situation in small systems such as Ala_{10}-Gly_5-Ala_{10}. One possible extension of the above ideas to "phase transitions" in biological molecules and other small systems is the classification scheme by Borrmann *et al.* [14]. In this approach one computes the discrete line density of zeros as an average of the inverse distances between neighboring zeros,

$$\phi(\tau_k) = \frac{1}{2}\left(\frac{1}{|\beta_k - \beta_{k-1}|} + \frac{1}{|\beta_{k+1} - \beta_k|}\right), \tag{14}$$

and approximates $\phi(\tau)$ by a simple power law $\phi(\tau) \sim \tau^\alpha$. Taking the first four complex zeros, one obtains

$$\alpha = \frac{\ln \phi(\tau_3) - \ln \phi(\tau_2)}{\ln \tau_3 - \ln \tau_2}. \tag{15}$$

With a second parameter γ, related to the crossing angle of this line with the real axis,

$$\gamma = [\mathrm{Re}(\beta_2) - \mathrm{Re}(\beta_1)]/(\tau_2 - \tau_1), \tag{16}$$

and following the classification scheme by Grossmann and Rosenhauer [24,25], phase transitions can now be classified according to the values of these two parameters: for $\alpha \leq 0$ and $\gamma = 0$ one has a phase transition of first order, it is of second order if $0 < \alpha < 1$ and arbitrary γ, and for $\alpha > 1$ and arbitrary γ one has a higher order transition. We have

evaluated the usefulness of this approach both for spin systems and polyalanine chains [26,27]. Preliminary results for Ala_{10}-Gly_5-Ala_{10} are also listed in Ref. [27].

For Ala_{10}-Gly_5-Ala_{10}, we find two lines of complex zeros. The corresponding first four zeros for each characteristic line are listed in Table 2. Our error estimate is based on the jackknife method [28] with 16 bins. These lines lead to two critical temperatures $T_{hc} = 480$ K and $T_f = 271$ K (estimated from the real part of β) that agree with the corresponding values $T_{hc} = 483 \pm 8$ K and $T_f = 265 \pm 7$ K found by us above with different methods.

Using these zeros we have calculated the parameters α and γ that characterize in the Borrmann *et al.* approach phase transitions in small systems. For the first transition, at $T = 480$ K, we find $\alpha = 1.1(1.5)$ and $\gamma = -0.4(2)$. The errors reflect large fluctuations in the values of the two parameters α and γ that do not allow us to determine whether the helix-coil transition is a weak first order or a strong second order phase transition. This problem was also observed in our earlier work on polyalanine [9,26] where we were also not able to establish clearly the order of the helix-coil transition. However, our results illustrate the strength of this transition that also leads to the pronounced peak in the specific heat observed in Fig. 3, and suggest a nucleation mechanism for α-helix formation. Our data are more decisive in the case of the second transition, at $T = 265$ K, which marks the collapse and folding of the peptide. Here we find $\alpha = 0.32(8)$ and $\gamma = 0.36(2)$. These values indicate a second-order transition which is consistent with what one would expect for a transition between extended and compact structures and imply that collapse and folding of the Ala_{10}-Gly_5-Ala_{10} is connected with long range correlations between the residues.

Our above analysis of the thermodynamics of our peptide suggests that Ala_{10}-Gly_5-Ala_{10} folds in a 2 step process. The first step is the formation of α-helices and can be characterized by a helix-coil transition temperature $T_{hc} = 483 \pm 8$ K. The formation of α-helices then restricts the possible configuration space. Energetically most favorable is the folding of two α-helices (made out of the alanine residues) into a hairpin. This second step can be characterized by a lower folding temperature $T_f = 265 \pm 7$ K. Note that this folding temperature is in the biological relevant temperature regime while helix-formation can also happen at much higher temperatures. The above described two step folding of our artificial peptide is reminiscent of the well known framework [29,30] and collision-diffusion model [31] of folding which also propose that local elements of native local secondary structure form independently of tertiary structure. These elements diffuse until they collide and coalesce to give a tertiary structure. In our case, the temperature region of $265 - 480$ K is the one where the thermal energy of the molecule does not allow coalescing of the helix-fragments that therefore form and decay. Some stabilization happens when these fragments try to form one extended helix, however, the inherent flexibility of the glycine residues, connecting the two alanine chains, and the gain in Lennard-Jones energy lead instead at temperatures below T_f to a U-turn-like bundle of two (antiparallel) α-helices connected by a turn of glycine residues as the most stable structure. Note that this picture is consistent with energy landscape theory and funnel concept [2,3]. Fig. 5b depicts the appearance of a folding funnel at $T = 270$ K towards our "native structure" 'A'. The competing structure 'B', that at this temperature has a slightly higher ($\approx 1 k_B T$) free energy (see the 1 $k_B T$ contour line for structure 'A' that is missing for conformer 'B'), acts as a local trap. However, the free energy barriers of ≈ 6 $k_B T$ can be overcome at this temperature by thermal fluctuations. Below that temperature the relative weight of structure 'B' decreases (see Fig.7) and its free energy difference to 'A' increases: the energy landscape becomes even more funnel like (data not shown). The energy landscape of Fig. 5b allows for a multitude of folding pathways that all, however, follow the above described two-step process.

An interesting question is how general the above obtained results are. A direct comparison with experimental data is difficult since solvent effects were neglected in the simulation of Ala_{10}-Gly_5-Ala_{10} and most experiments study solvated peptides. An exception are the techniques developed by Jarrold and collaborators for examination of gas-phase conformations of proteins and peptides [32]. An experimental study of Ala_{10}-Gly_5-Ala_{10} using these techniques is now planed. The authors are not aware of experimental results for the solvated peptide. In order to compare our work with experiments of other short helical peptides [33,34], we therefore started now simulations of Ala_{10}-Gly_5-Ala_{10} where the solvation effects are approximated by a solvent accessible surface term [35]. This will allows us also to test the dependency of our results on the solvation model. Simulating another, slightly more complicated, artifical peptide, Ala_{10}-Gly_5-Ala_{10}-Gly_5-Ala_{10} that presumably will fold in a three-helix bundle, will allow in addition a direct comparison with recent experimental work by Myers and Oas [34] where the relation between helix-formation and folding was studied for the 58-residue B domain of protein A.

IV. CONCLUSION

In summary, we have performed multicanonical simulations with high statistics of a simple artificial peptide, the 25 residue Ala_{10}-Gly_5-Ala_{10}. We found that this peptide folds into a specific structure that is determined solely by the intrinsic properties of the molecule (since solvent interactions are absent in our simulations. In gas-phase, the

peptide exhibits two characteristic transitions. At $T_{hc} = 483 \pm 8$ K we observed a helix-coil transition that is either a weak first order transition or a strong second order transition. Our results indicate that there is a second transition at $T_f = 265 \pm 7$ K, the folding transition, that is second order-like. These results suggest that folding of this peptide in gas-phase is a two-step process. In a first step, the alanine residues form independently helical segments which then afterwards in a second step assemble to a U-turn like structure of two antiparallel α-helices connected by a turn. By using an implicit solvent model in our simulations we started now to investigate whether the final structure or this two-step process changes in the present of water.

Acknowledgements:
U. Hansmann gratefully acknowledges support by a research grant from the National Science Foundation (CHE-9981874), and N.A. Alves support by CNPq (Brazil).

---

[1] C.B. Anfinsen, *Science* **181**, 223 (1973).
[2] J.D. Bryngelson and P.G. Wolynes, *Proc. Natl. Acad. Sci. (USA)* **84**, 7524 (1987).
[3] J.N. Onuchic, Z. Luhey-Schulten and P.G. Wolynes, *Annu. Rev. Phys. Chem.* **48**, 545 (1997).
[4] U.H.E. Hansmann, Y. Okamoto and J.N. Onuchic, *Proteins* **34**, 472 (1999).
[5] U.H.E. Hansmann and J.N. Onuchic, *J. Chem. Phy.* **115**, 1601 (2001).
[6] D. Poland and H.A. Scheraga, *Theory of Helix-Coil Transitions in Biopolymers* (Academic Press, New York, 1970).
[7] J.P. Kemp and Z.Y. Chen, *Phys. Rev. Lett.* **81**, 3880 (1998).
[8] U.H.E. Hansmann and Y. Okamoto, *J. Chem. Phys.* **110**, 1267 (1999); **111** (1999) 1339(E).
[9] N.A. Alves and U.H.E. Hansmann, *Phys. Rev. Lett.* **84**, 1836 (2000).
[10] N.A. Alves and U.H.E. Hansmann, *Physica A* **292**, 509 (2001).
[11] A. Mitsutake and Y. Okamoto, *J. Chem. Phys.* **112**, 10638 (2000).
[12] Y. Peng and U.H.E. Hansmann, *Solvation model dependency of helix-coil transition in polyalanine*, *Biophysical J.* (2002), in press.
[13] B.A. Berg and T. Neuhaus, *Phys. Lett.* B **267**, 249 (1991).
[14] P. Borrmann, O. Mülken and J. Harting, Phys. Rev. Lett. 84 (2000)3511; O. Mülken, P. Borrmann, J. Harting and H. Stamerjohanns, Phys. Rev. A64 (2001) 013611; O. Mülken and P. Borrmann, Phys. Rev. C63 (2001) 024306.
[15] K.R. Shoemaker, P.S. Kim, E.J. York, J.M. Stewart, R.L. Baldwin, *Nature* **326**, 563 (1987).
[16] M.J. Sippl, G. Némethy, and H.A. Scheraga, *J. Phys. Chem.* **88**, 6231 (1984), and references therein.
[17] F. Eisenmenger, U.H.E. Hansmann, Sh. Hayryan, C.-K. Hu, *Comp. Phys. Comm.* **138**, 192 (2001).
[18] U.H.E. Hansmann and Y. Okamoto, *Curr. Opin. Struc. Biol.* **9**, 177 (1999).
[19] U.H.E. Hansmann and Y. Okamoto, J. Comp. Chem. **14**, 1333 (1993).
[20] U.H.E. Hansmann and Y. Okamoto, in: Stauffer, D. (ed.) "*Annual Reviews in Computational Physics VI*" (Singapore: World Scientific), p.129. (1998).
[21] A.M. Ferrenberg and R.H. Swendsen, *Phys. Rev. Lett.* **61**, 2635 (1988); *Phys. Rev. Lett.* **63**, 1658(E) (1989), and references given in the erratum.
[22] B.A. Berg, *J. Stat. Phys.* **82**, 323 (1996).
[23] Y. Okamoto and U.H.E. Hansmann, J. Phys. Chem. **99**, 11276 (1995).
[24] S. Grossmann and W. Rosenhauer, Z. Physik 207 (1967)138.
[25] S. Grossmann and W. Rosenhauer, Z. Physik 218 (1969)437; S. Grossmann and W. Rosenhauer, Z. Physik 218 (1969)449.
[26] N.A. Alves, J.P.N. Ferrite and U.H.E. Hansmann, *Phys. Rev. E* **65**, 036110 (2002).
[27] N.A. Alves, U.H.E. Hansmann and Y. Peng, *Int. J. Mol. Sci.* **3**, 17 (2002).
[28] R.G. Miller, *Biometrika* **61**, 1 (1974).
[29] O.B. Ptitsyn, *Protein Eng.* **7**, 593 (1994).
[30] P.D. Kim and R.L. Baldwin, *Annu. Rev. Biochem.* **59**, 631 (1990).
[31] M. Karplus and D.L. Weaver, *Protein Sci.* **3**, 650 (1994).
[32] R.R. Hudgins, M.A. Ratner and M.F. Jarrold, *J. Am. Chem. Soc.* **120** 12974 (1998).
[33] E.M. Boczko and C.L. Brooks III, *Science* **269**, 393 (1995).
[34] J.K. Myers and T.G. Oas, *Nat. Str. Bio.* **8** 552 (2001).
[35] U.H.E. Hansmann, in preparation.

Table I. Dihedral angles for the two configurations shown in Fig. 5

State	Conformer A			Conformer B		
E_{tot} (Kcal/mol)	-34.7			-23.9		
Residue	ϕ	ψ	χ	ϕ	ψ	χ
Ala-1	-101.7	154.4	-178.1	-55.2	-54.9	61.5
Ala-2	-65.4	-35.5	-173.8	-70.6	-37.8	49.2
Ala-3	-68.2	-36.1	-61.7	-60.4	-30.8	-178.3
Ala-4	-70.6	-39.0	-69.7	-78.6	-37.6	-43.4
Ala-5	-64.3	-40.6	-54.1	-66.5	-28.8	176.5
Ala-6	-66.3	-38.3	175.1	-70.6	-50.4	-55.8
Ala-7	-69.5	-31.9	-172.6	-64.2	-32.6	-178.6
Ala-8	-75.5	-31.6	57.2	-68.6	-43.4	-58.3
Ala-9	-62.6	-45.2	-172.9	-67.8	-41.0	-164.8
Ala-10	-73.4	-54.4	-59.0	-60.8	-43.3	53.4
Gly-11	-91.9	65.0		-64.3	-40.5	
Gly-12	156.2	-80.6		-64.9	-44.9	
Gly-13	151.5	-176.6		-64.6	-47.0	
Gly-14	-60.1	-35.5		-63.0	-33.0	
Gly-15	-63.5	-38.0		-72.6	-39.9	
Ala-16	-72.6	-34.6	-48.7	-70.3	-31.1	83.1
Ala-17	-69.4	-32.9	-52.2	-69.2	-39.2	63.3
Ala-18	-70.2	-38.4	-53.6	-68.4	-39.9	63.8
Ala-19	-70.5	-35.1	174.4	-66.1	-38.7	-58.5
Ala-20	-66.6	-40.4	179.5	-67.1	-41.9	-170.9
Ala-21	-68.7	-40.3	173.3	-66.0	-33.3	66.1
Ala-22	-61.2	-36.0	61.7	-73.9	-35.5	61.9
Ala-23	-71.1	-52.6	-51.3	-65.2	-37.8	-176.5
Ala-24	-153.3	111.8	58.6	-73.0	-39.3	-39.5
Ala-25	-62.8	-62.6	-173.5	-69.5	-8.8	71.0

Table II. Partition function zeros for the two transitions observed for Ala_{10}-Gly_5-Ala_{10}.

Re(β_1)	τ_1	Re(β_2)	τ_2	Re(β_3)	τ_3	Re(β_4)	τ_4
1.0463(46)	0.1307(53)	1.0144(99)	0.2112(55)	1.051(44)	0.310(36)	1.055(46)	0.347(41)
1.855(21)	0.263(12)	1.991(25)	0.637(41)	2.057(53)	0.923(43)	2.070(43)	1.229(55)

Figure Captions:

Fig. 1 The average helicity $< n_H > (T)$ of Ala_{10}-Gly_5-Ala_{10} as a function of temperature T. The corresponding values of the susceptibility $\chi(T)$ are ploted in the inset. Our data rely on a single multicanonical simulation of 8,000,000 Monte Carlo sweeps.

Fig. 2 The average ECEPP/2 energy $< E_{tot} >$ and the corresponding partial energy terms, Coulomb energy $< E_C >$, Lennard-Jones term $< E_{LJ} >$, hydrogen-bond energy $< E_{hb} >$ and torsion energy $< E_{tor} >$, as a function of temperature T for Ala_{10}-Gly_5-Ala_{10}.

Fig. 3 The specific heat $C(T)$ of Ala_{10}-Gly_5-Ala_{10} as a function of temperature T.

Fig. 4 The average end-to-end distance $< d_{e-e} > (T)$ as a function of temperature T for Ala_{10}-Gly_5-Ala_{10}.

Fig. 5 Free energy landscape of Ala_{10}-Gly_5-Ala_{10} as a function of helicity n_H and end-to-end distance d_{e-e} at temperature (a) $T_{hc} = 480$ K and (b) $T_f = 270$ K. The contour lines are drawn in multiples of k_BT indicated in the key.

Fig. 6 Lowest-energy conformation 'A' of Ala_{10}-Gly_5-Ala_{10} (a) and the conformation 'B' (which has the largest helicity) (b) as found in our multicanonical simulation of 8,000,000 Monte Carlo sweeps.

Fig. 7 Relative weight of the lowest-energy conformation 'A' and conformation 'B' (which has maximal helicity) as a function of temperature.

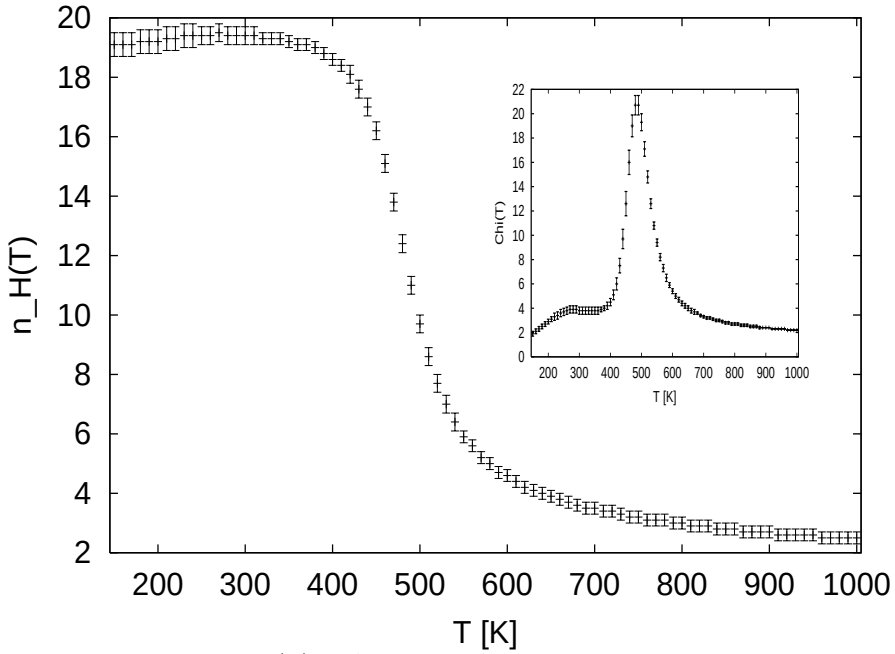

(Fig.1) 1. The average helicity $< n_H > (T)$ of Ala_{10}-Gly_5-Ala_{10} as a function of temperature T. The corresponding values of the susceptibility $\chi(T)$ are ploted in the inset. Our data rely on a single multicanonical simulation of 8,000,000 Monte Carlo sweeps.

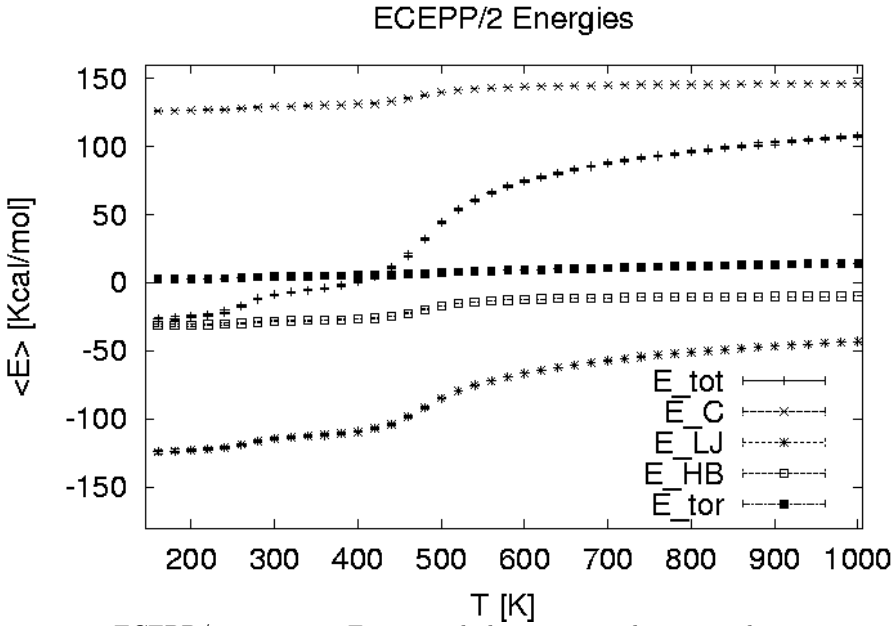

(Fig.2) 2. The average ECEPP/2 energy $< E_{tot} >$ and the corresponding partial energy terms, Coulomb energy $< E_C >$, Lennard-Jones term $< E_{LJ} >$, hydrogen-bond energy $< E_{HB} >$ and torsion energy $< E_{tor} >$, as a function of temperature T for Ala_{10}-Gly_5-Ala_{10}.

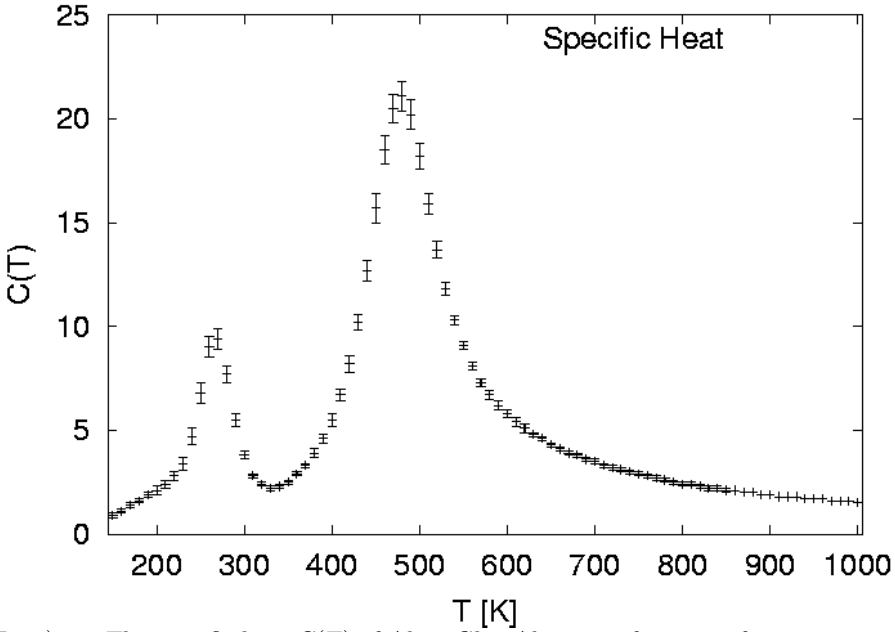

(Fig.3) 3. The specific heat $C(T)$ of Ala_{10}-Gly_5-Ala_{10} as a function of temperature T.

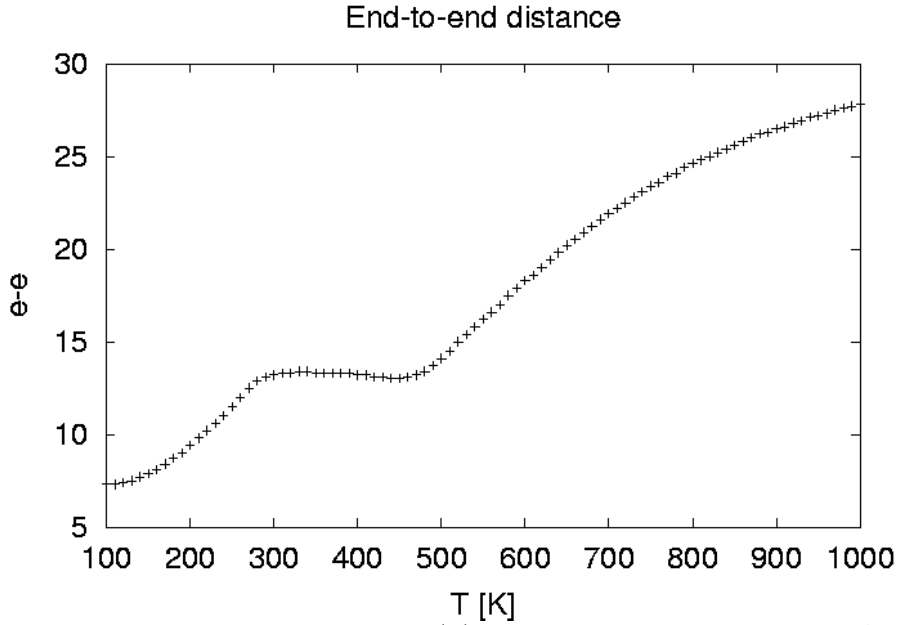

(Fig.4) 4. The average end-to-end distance $< d_{e-e} > (T)$ as a function of temperature T for Ala_{10}-Gly_5-Ala_{10}.

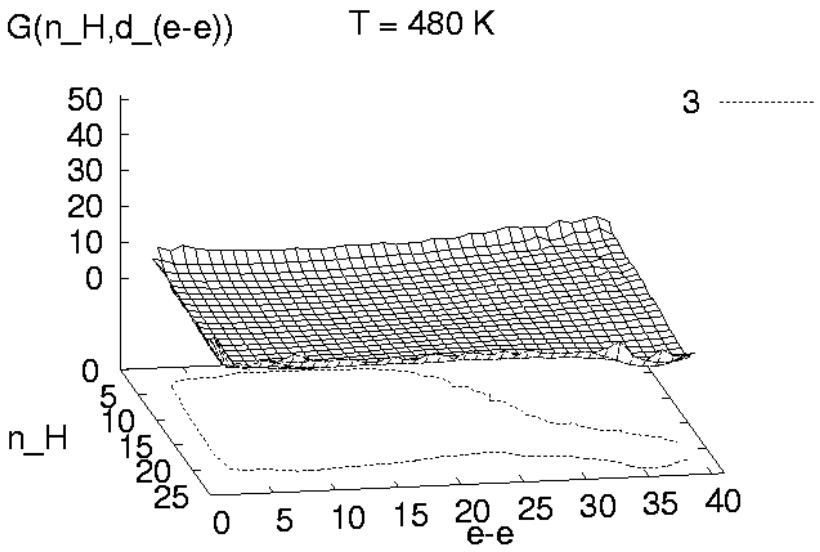

(Fig.5a) 5. Free energy landscape of Ala_{10}-Gly_5-Ala_{10} as a function of helicity n_H and end-to-end distance d_{e-e} at temperature (a) $T_{hc} = 480$ K and (b) $T_f = 270$ K.

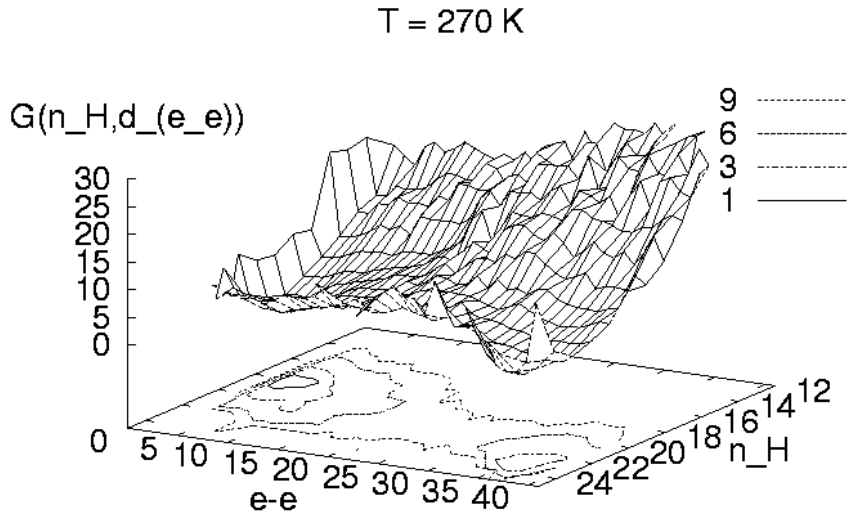

(Fig.5b) 6.

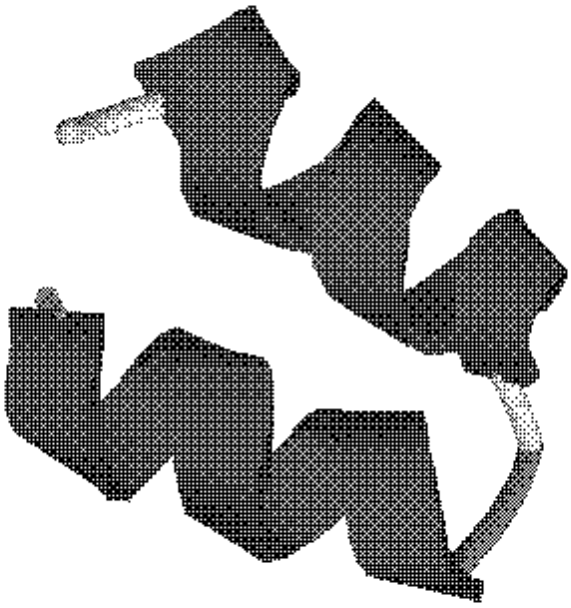

(Fig.6a) 7. Lowest-energy conformation 'A' of Ala_{10}-Gly_5-Ala_{10} (a) and the conformation 'B' (which has the largest helicity) (b) as found in our multicanonical simulation of 8,000,000 Monte Carlo sweeps.

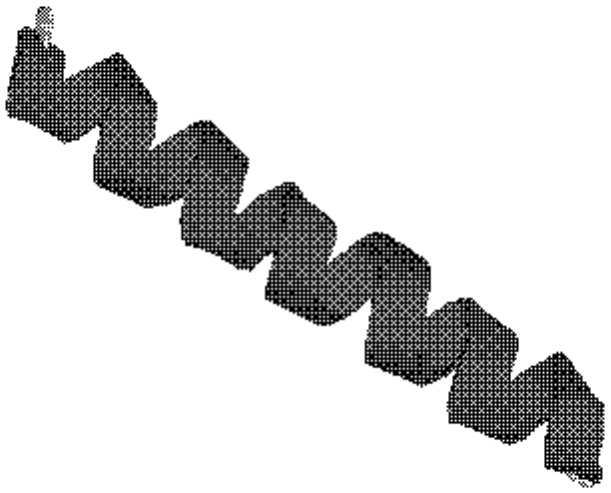

(Fig.6b) 8.

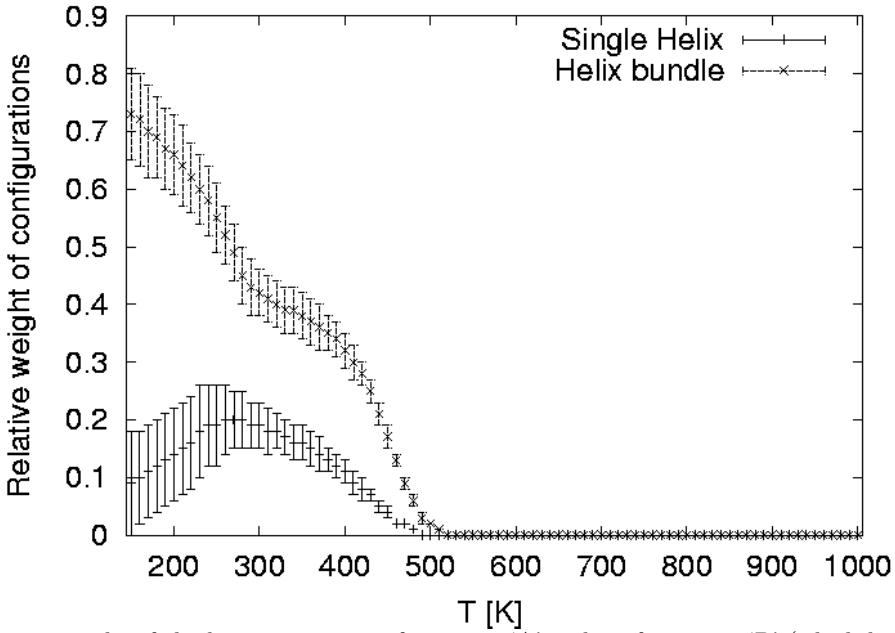

(Fig.7) 9. Relative weight of the lowest-energy conformation 'A' and conformation 'B' (which has maximal helicity) as a function of temperature.